Solar and Stellar Coronal Mass Ejections
Proceedings of the IAU Symposium No. 388, 2024
N. Gopalswamy, O. Malandraki, A. Vidotto & W. Manchester, eds.
doi:10.1017/xxxxx

The Role of Magnetic Reconnection in the Structure & Dynamics of Fast Coronal Mass Ejections

Brian T. Welsch[1] **& C. R. DeVore**[2]

[1]Natural & Applied Sciences, University of Wisconsin - Green Bay,
2420 Nicolet Drive, Green Bay, WI 54311, USA
[2]Heliophysics Science Division, NASA Goddard Space Flight Center,
8800 Greenbelt Road, Greenbelt, MD 20771, USA

Abstract. Both observations and models of flare-associated coronal mass ejections (CMEs) suggest that magnetic reconnection in an ejection's wake substantially increases the net, outward Lorentz force accelerating the CME. A stronger outward force can cause a feedback loop, driving further magnetic reconnection in a "reconnective instability." The flux accretion model captures this by relating reconnected flux, $\Delta\Phi_{\rm rec}$, and magnetic field strength, $B_{\rm CME}$, to increased outward Lorentz force, ΔF_r. To better understand reconnection's role in CME dynamics, we analyze two snapshots from a 2.5D, MHD simulation of a breakout eruption. Outward Lorentz forces increase substantially as reconnection proceeds, caused primarily by "flank currents," which flow just inside the boundary of the rising ejection's wake and parallel to its axis. This model's reconnection jet also alters the ejection's internal structure, an effect that could be sought in observations. Analyzing reconnection-induced Lorentz forces in 3D simulations could provide additional insights into CME dynamics.

Keywords. Magnetic Reconnection, CMEs – dynamics, CMEs – structure, CMEs – acceleration

1. Introduction

Magnetic reconnection is a rich topic (e.g., Priest and Forbes 2000) that is relevant to magnetic energy release in plasmas of the Sun, other stars, and many other physical systems. In the case of solar flares, reconnection is widely believed to be the central process facilitating the release of stored magnetic energy (e.g., McKenzie 2002). For a flare-associated coronal mass ejection (CME), *flare reconnection* (Antiochos et al. 1999) is believed to occur in the wake of the rising ejection. Antiochos et al. (1999) contrast flare reconnection with *breakout reconnection*, which occurs in front of the erupting structure, and which they posit initiates the eruption by removing overlying, restraining flux. Lin and Forbes (2000) analyzed a 2.5D, Cartesian model of a CME, and describe a feedback loop between flare reconnection and the upward force accelerating the CME. Moore et al. (2001) proposed that the eruption is initiated by *tether cutting* reconnection under the pre-eruptive structure, which reduces the effect of downward magnetic tension from fields overlying that structure. Once an eruption is underway, tether cutting reconnection and flare reconnection are indistinguishable.

Observationally, significant correlations have been found between CMEs' speeds, $v_{\rm CME}$, and the amounts of magnetic flux that reconnected in their associated flares, $\Phi_{\rm rec}$, deduced from flare ribbons Qiu and Yurchyshyn (2005) or post-eruption arcades Gopalswamy et al. (2017). These correlations suggest, consistent with the theoretical models above, that reconnection plays an important role in altering the forces on ejections. From the temporal correlation between soft X-ray emission, interpreted as a proxy of magnetic reconnection, and CME acceleration, Zhang and Dere (2006) also suggested that reconnection and CME acceleration operate in a feedback loop early in the eruption process: more reconnection drives more acceleration, which in turn drives further reconnection, and further subsequent acceleration.

Based upon these and other observations and models, Welsch (2018) presented the *flux accretion* model of eruptions, in which flare reconnection below a rising ejection adds magnetic flux to the ejection. This (i) leads to momentum transfer from the outflow jet to the ejection and (ii) increases the net, outward component of the Lorentz force,$(\mathbf{J}\times\mathbf{B})/c$, acting on the .ejection. In the model's treatment of Lorentz forces, the accreted underlying flux both reduces the net force due to downward magnetic tension from overlying fields (the mechanism of tether cutting) and increases the outward hoop force (e.g., Chen 1996) from these underlying fields exerting greater outward magnetic pressure on the ejection. For both components of the total force, the flux accretion model predicts that the change in outward force, ΔF_r, due to the reconnection of an amount of flux $\Delta\Phi_{\rm rec}$ scales as

$$\Delta F_r \propto \Delta\Phi_{\rm rec} B_{\rm CME} \ , \tag{1}$$

where $B_{\rm CME}$ is a characteristic field strength in the vicinity of the CME.

In this brief paper, we explore how reconnection affects the Lorentz force on models of CMEs. In Section 2, we consider a highly idealized model of magnetic fields and currents in a CME source region, and analyze the effect of reconnection upon these fields and currents. Then, in Section 3, we quantitatively investigate evolution of the Lorentz forces — and the magnetic fields and currents that contribute to it — in two snapshots from a numerical simulation of CME as flare reconnection proceeds.

2. Qualitative Analysis of Reconnection's Effect on Lorentz Forces

We first consider the overall structure of the magnetic field and currents in a generic eruptive configuration, and then consider how these are relevant for flare reconnection and evolving Lorentz forces during the eruption. To illustrate the large-scale morphology of the system, Figure 1 shows a snapshot from the axisymmetric, 2.5D MHD simulation that we will analyze in the next section. (Details of the simulation are described there.) The simulation employed spherical coordinates, and we interpolated its physical values onto a uniform, Cartesian, (1024 $\times$ 1024) grid, with $x\in[0,6]R_\odot$ and $z\in[-3,3]R_\odot$. The simulation's inner boundary, at $r=R_\odot$, corresponds to the base of the corona and can be seen near the image's left edge. Co-latitude θ increases clockwise from the Sun's north pole (out of the frame, at $z=+1$) toward its equator (at $z=0$), and ϕ increases into the page. The grayscale shows B_ϕ, weighted by r^2 so its structure remains visible even as it weakens with larger r. The black lines show contours of the flux function, f, with the poloidal field, $\mathbf{B}_{\rm pol}$, obeying

$$\mathbf{B}_{\rm pol} = \nabla f \times \nabla\phi \ , \tag{2}$$

meaning contours of f correspond to field lines of $\mathbf{B}_{\rm pol}$. For $x\in[1.25,2.5]R_\odot$, this flux system's radial field is outward below the $z=0$ line and inward above it. An intense azimuthal current — a large-scale current sheet — flows between these oppositely directed radial fields, and is directed out of the page. In Figure 1, this current is concentrated between the innermost flux function contours straddling $z=0$. The red and blue contours bracketing $(x,z)=(1.7,0)$ correspond to 100 km/s inward and outward radial outflows, respectively, from the flare reconnection region.

An eruptive flare invariably occurs above a photospheric polarity inversion line (PIL), across which radial photospheric magnetic field changes sign. The horizontal photospheric field along a flaring PIL almost always exhibits a significant *shear* component, i.e., a component of $\mathbf{B}$ parallel to the PIL. Associations between magnetic shear and flare occurrence were noted long ago (e.g., Hagyard et al. 1984). In addition to being flare-prone, sheared fields along PILs have also been associated with increased likelihood of CME occurrence (e.g., Falconer 2001; Falconer et al. 2003). Typically, sheared fields are localized in the vicinity of PILs, with horizontal photospheric fields farther from PILs exhibiting less shear (e.g., Falconer 2001).

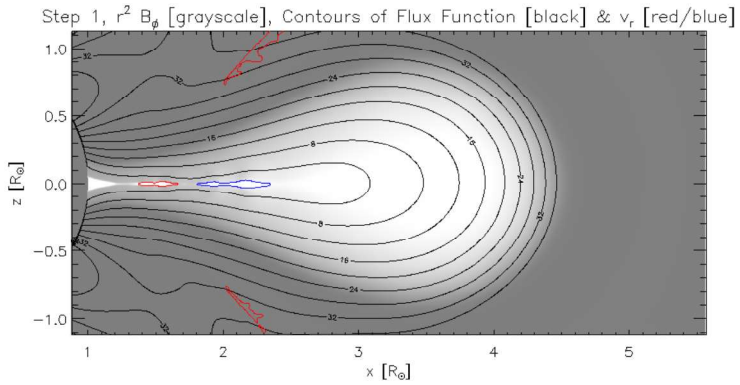

Figure 1. In this snapshot from the spherical, axisymmetric, 2.5D MHD simulation that we analyze, the simulation's spherical inner boundary ($r = R_\odot$) can be seen at frame left, x increases to the right, θ increases clockwise from the Sun's north pole (out of the frame, at $z = +1$) toward its equator (at $z = 0$), and ϕ increases into the page. The grayscale shows B_ϕ, weighted by r^2 to keep the structure of B_ϕ visible as it weakens with increasing r. The red and blue contours correspond to 100 km/s inward and outward radial velocities, respectively. The black lines show contours of the flux function, f, corresponding to poloidal projections of field lines.

This decrease in shear with distance from the PIL is also typically observed in overlying fields, inferred from the directions of chromospheric H-α fibrils and coronal loops' axes.

Because the coronal plasma in CME source regions is magnetically dominated (the plasma's β, its ratio of gas to magnetic pressures, is much less than unity), the $(\mathbf{J} \times \mathbf{B})/c$ (Lorentz) force is very small in slowly evolving, pre-eruptive fields, i.e., such fields are very nearly *force-free*. Thus, (i) $\mathbf{J} \neq 0$ implies that $\mathbf{J}$ must flow very nearly parallel to $\mathbf{B}$, and (ii) the presence of a significant shear component of $\mathbf{B}$ implies a shear component of $\mathbf{J}$. The localization of the shear component of $\mathbf{B}$ in the vicinity of the PIL implies that there must also be a current sheath surrounding the sheared field, to isolate or "switch off" the shear component of $\mathbf{B}$. These elements are illustrated in the left panel Figure 2, which shows an overhead view of magnetic structure near a sheared photospheric PIL (red dashed line). The red lines with arrows show magnetic fields above the photosphere, with lines progressing from thicker to thinner with increasing height. The red $\odot$ and $\otimes$ show the polarity of the photospheric radial magnetic field. The blue $\odot$ and $\otimes$ symbols show the sheath current (similar to that in a solenoid) that isolates the magnetic field's shear component (which points to the right).

Flare reconnection alters the connectivity of both preflare coronal magnetic fields and current structures. We are primarily interested in how reconnection alters the radial component of

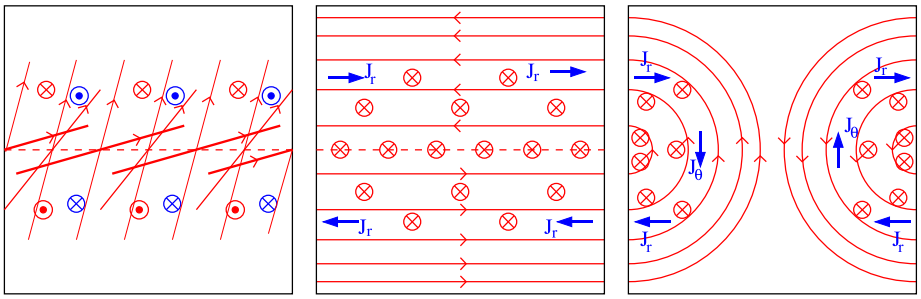

Figure 2. Left: An overhead view of magnetic structure near a sheared photospheric PIL (red dashed line). Solid red lines with arrows show magnetic fields above the photosphere, with thicker to thinner corresponding to fields at increasing altitudes. Red $\odot$ and $\otimes$ show polarity of the photospheric radial magnetic field. Blue $\odot$ and $\otimes$ symbols show the sheath current that isolates (or "switches off") the magnetic field's shear component (which points to the right). Middle: This side view, above and along the PIL from the left panel, shows flare reconnection, in which oppositely directed magnetic field components in the corona (solid red lines) reconnect across a current sheet (dashed red line, with its current directed out of the page) in the presence of guide field (red $\otimes$ symbols). Sheath currents associated with the localization of the guide field are also present (blue vectors). Right: Reconnection joins formerly oppositely directed fields into arched fields (solid red lines), and in the process reroutes the sheath currents (blue vectors), introducing oppositely directed currents between the post-reconnection flux systems. Each of these field and current components can, in principle, contribute to the radial Lorentz force that accelerates the ejection.

the Lorentz force, F_r,

$$cF_r = J_\theta B_\phi - J_\phi B_\theta \ . \tag{3}$$

Current in the reconnecting current sheet (which we assume is thin, but not infinitely so) also flows parallel and above to the PIL; in our geometry, this is J_ϕ. The shear component of **B** corresponds to a guide field, i.e., a nonzero field component along the reconnecting current sheet (see, e.g., Priest and Forbes 2000); in our geometry, this is B_ϕ. Reconnection in the presence of a guide field can introduce twist into originally untwisted fields (e.g., Wright and Berger 1989; Chae 1999). The resulting fields can be highly twisted (e.g., Longcope et al. 2007) and generally carry currents. Aspects of the reconfiguration of coronal fields and current components are illustrated schematically in the middle and right panels of Figure 2. These panels depict a view in the corona along the guide field (i.e., above and along the PIL in the Figure's left panel), showing the reversed field components that reconnect (solid red lines), the guide field (red $\otimes$ symbols), and the sheath currents (blue vectors) associated with the localization of the shear component of **B**. In the middle panel, a current sheet exists along the red dashed line, with current flowing out of the page. Reconnection joins oppositely directed fields (solid red lines in middle panel) into arched fields (solid red lines in right panel), which possess a B_θ component in our geometry. The process also reroutes the sheath currents (blue vectors), introducing oppositely directed currents between the post-reconnection flux systems, corresponding to a J_θ component. The repulsion of these antiparallel J_θ currents works against the attraction of the parallel J_ϕ currents in the post-reconnection fields (both out of the page here).

In the following section, we investigate the evolution of F_r as flare reconnection proceeds in the model CME, and compare the contributions from the $(J_\theta B_\phi)$ and $(J_\phi B_\theta)$ terms in Equation (3).

3. Quantitative Analysis of Reconnection's Effect on Lorentz Forces

In this section, we analyze two snapshots from a 2.5D, axisymmetric, breakout simulation using the Adaptively Refined Magnetohydrodynamic Solver (ARMS) that closely matches the simulations performed and analyzed by Karpen et al. (2012) (hereafter "KAD12"). The run analyzed here differs in only one potentially relevant detail: in the simulations that we analyze, six levels of grid refinement were permitted, whereas only five levels were enabled in KAD12. The first snapshot, our Step 1 (the code's step 241354), corresponded to the onset of flare reconnection, and at the second snapshot, our Step 2 (the code's step 254006), a substantial amount of flux has reconnected. (Data from additional time steps could be analyzed, but computation of the flux function for this simulation must be done *post facto*, which requires significant manual effort. Consequently, the analysis of additional data would require the availability of additional resources.)

Figure 3 shows the inward and outward (red and blue, respectively) components of the radial Lorentz force at each step, both heavily saturated and weighted by r^4, so their spatial structure can be discerned at large r, despite $\mathbf{J}$ and $\mathbf{B}$ being much weaker there than near $r = R_\odot$. The thin black contours show the flux function, which makes clear that a substantial amount of flux has reconnected between these snapshots. The thick contour outlines a *CME mask*, meant to capture the main body of the erupting structure. We have chosen to define this mask using a fixed-r inner boundary and an outer boundary set at the same flux-function contour in both snapshots. We also note the presence of several key structural features of the global magnetic field. Post-reconnection, poloidal fields in the flare arcade are prominent near $z = 0$ and $x \in [1, 1.5]R_\odot$ in the bottom panel. The breakout current sheet is near $x = 5R_\odot$ in the top panel. The separatrix current sheets, which flow between the erupting flux system and adjacent systems and are extensions of the breakout current sheet, run diagonally near $1.5R_\odot < x < 2.25R_\odot$ in both panels.

The distribution of the radial Lorentz force is richly structured, with features in the reconnection outflow region clearly making large contributions to the Lorentz force. Notably, forces present in the jet are strong enough to deform post-reconnection flux-function contours, making them concave inward — i.e., with a magnetic tension that points radially inward. It is unclear whether observed CMEs exhibit such structure. To quantify evolution of the radial Lorentz force as the reconnection proceeds, we can integrate the interpolated force density over the CME mask on our Cartesian grid, weighted by r (since $dV = dx\,dz\,r\,d\phi$, as in cylindrical coordinates). Applying the Step-1 mask to both steps, the outward Lorentz force increases by a factor of 2.3; applying the Step-2 mask to both steps, the outward Lorentz force increases by a factor of 1.4; and applying the Step-1 mask at Step 1 and the Step-2 mask at Step 2 (i.e., advecting the flux-function boundary), the outward Lorentz force increases by a factor of 1.5. Expansion of the eruption, combined with conservation of flux, weakens its magnetic field: we averaged each step's $|\mathbf{B}|$ over the CME mask at that step, and this average decreases by about 20% between Steps 1 and 2. (The area of Step 2's mask is 5/3 the size of Step 1's.) All else equal, a weaker $|\mathbf{B}|$ would decrease the Lorentz force. However, the average current density, $|\mathbf{J}|$, in Step 2's CME mask is about 4/3 that in Step 1's. This increase in Lorentz force can be explained both by reconnection and the development of an ideal MHD instability, e.g., the torus instability (Kliem and Török 2006).

In Figure 4, we investigate the radial profile of the radial component of the Lorentz force, $cF_r = (J_\theta B_\phi - J_\phi B_\theta)$, outward from the flare reconnection site in Steps 1 and 2. To compare contributions to F_r between small and large r, we weight all quantities plotted by r^2. The flare reconnection site was identified in each step by finding where the smoothed radial

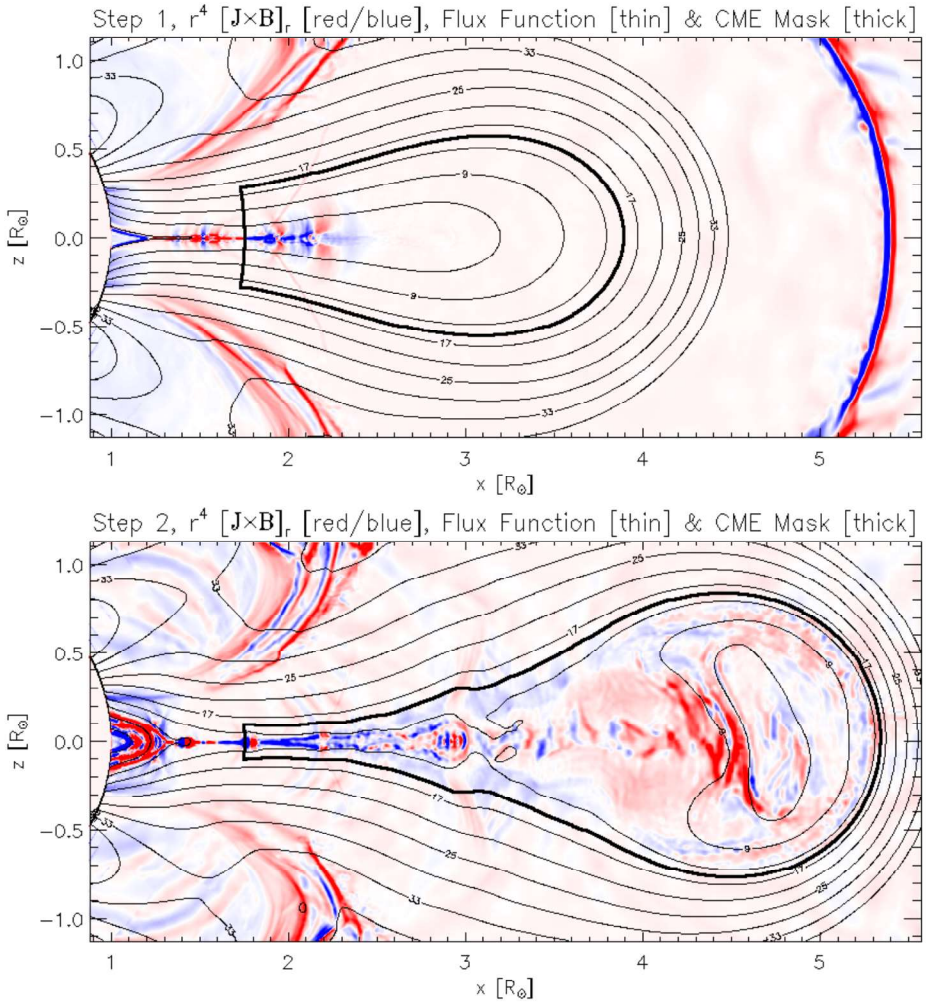

Figure 3. Red (blue) shows inward (outward) components of the radial Lorentz force at snapshots 1 and 2, weighted by r^4, so their spatial structure can be discerned at large r, where **J** and **B** are much weaker than near the model's inner boundary. The thin black contours show the flux function, from which evolution of the field, including some effects of reconnection, can be inferred. The thick contour shows a CME mask whose outer boundary is at the same flux-function contour in both snapshots (see text).

velocity along $z = 0$ changed sign. The values plotted in this figure are *strip-averaged*: to compute them, we averaged values of $[J_\theta B_\phi]$ and $-[J_\phi B_\theta]$ in a 100-cell-wide strip, encompassing $z \in [-0.29, 0.29] R_\odot$. The highly oscillatory structure of $r^2(J_\theta B_\phi - J_\phi B_\theta)$ in the top panel of Figure 4 precludes clearly identifying how the primary contributions to the overall force arise. To clarify which areas contribute to the CME's acceleration, in the middle panel, at each r we plot the *cumulative* (summed) value of $r^2(J_\theta B_\phi - J_\phi B_\theta)$, from the base of the reconnection

outflow to that r. In this cumulative plot, a positive (negative) slope over some interval in r indicates a net positive (negative) contribution to the CMEs outward acceleration in that interval. Clearly, Lorentz forces that develop in the reconnection jet begin making a much larger contribution to the CME's acceleration between Steps 1 and 2. These findings support the idea that reconnection plays a key role in the ejection's outward acceleration, consistent with the expectations of Lin and Forbes (2000) and Zhang and Dere (2006), and the findings of KAD12.

Crucially, by decreasing the width of the strip over which the inverse-density-weighted radial force is averaged, we found that essentially *all* of the excess contribution to the outward force for Step 2 compared to Step 1 comes from *flank currents* — the tilted, blue bands just inside the CME mask (bottom panel of Figure 3) for $r \in [2.5, 3.5]R_\odot$. These structures are reminiscent of the standing waves (slow-mode shocks) in the Petschek reconnection model (Petschek 1964), but are macroscopic regions instead of the idealized discontinuities in that model. We found that these regions contain strong azimuthal currents parallel to that in the flare reconnection sheet, i.e., out of the page, resulting from a strong $\partial B_r/\partial\theta$ near the CME mask boundary, in which B_r exterior to the CME decreases relative to B_θ within the CME. The associated component of the Lorentz force, proportional to $B_\theta \partial B_r/\partial\theta$, corresponds to a magnetic tension. One expected signature of the hoop force would be substantial outward magnetic pressure from the poloidal field over the trailing face of the ejection, i.e., a strong $\partial B_\theta/\partial r$ (which also contributes to J_ϕ). However, we see little evidence to support this expectation.

The inward contribution to acceleration in the interval around $x \in [3.5, 4.5]R_\odot$ in the middle panel of Figure 4 is perhaps due to inward magnetic tension from the concave-inward curvature of field lines near $z = 0$ in this range, as may be seen in the bottom panel of Figure 3. Farther from $z = 0$, curvature in these lines reverses, implying an outward magnetic tension that plausibly cancels much (or all) of this inward force.

Consistent with our finding about the significance of the flank currents, the bottom panel of Figure 4 compares the two contributions to the outward Lorentz force at Step 2, $[r^2 J_\theta B_\phi]$ (blue) and $[-r^2 J_\phi B_\theta]$ (red). (The sum of these terms yields the red curve in the top panel.) There is a clear tendency for these terms to have similar magnitude but opposite signs. Over many intervals, however, the outward force is dominated by $(-J_\phi B_\theta)$ — that is, the product of the component of the azimuthal current (the component of $\mathbf{J}$ along the PIL) and the reconnected component of the magnetic field. In contrast, the product of the guide magnetic field with the current component that is redirected by reconnection from the radial direction into the θ direction (blue vectors in the right panel of Figure 2) is smaller at this point in the simulation.

We also remark that the volume-integrated Lorentz force acting on a flux tube with field strength B and flux Φ over the segment containing the flank currents would, like the tension force analyzed by Welsch (2018), scale as $B\Phi$. Unlike that tension force, however, the force from flank currents would only act transiently over a given tube segment, as the bend propagates along the tube.

4. Summary & Prospects

We have considered the effect of reconnection on currents and magnetic fields in eruptive flares, to better understand (i) how reconnection modifies these components of the Lorentz force and thus (ii) how flare-associated CMEs are accelerated.

We were not able to analyze enough snapshots from available ARMS simulations to test the flux accretion model's scaling in Equation (1). The necessary analysis would require computing radial Lorentz force changes between several closely spaced simulation steps, with each time interval involving reconnection of a known amount of flux. If sufficient resources — essentially, funding — becomes available, such an analysis will be pursued.

We found that, in this simulation, PIL-aligned "flank" current structures in the reconnection outflow make the primary contribution to the total outward Lorentz force. These findings

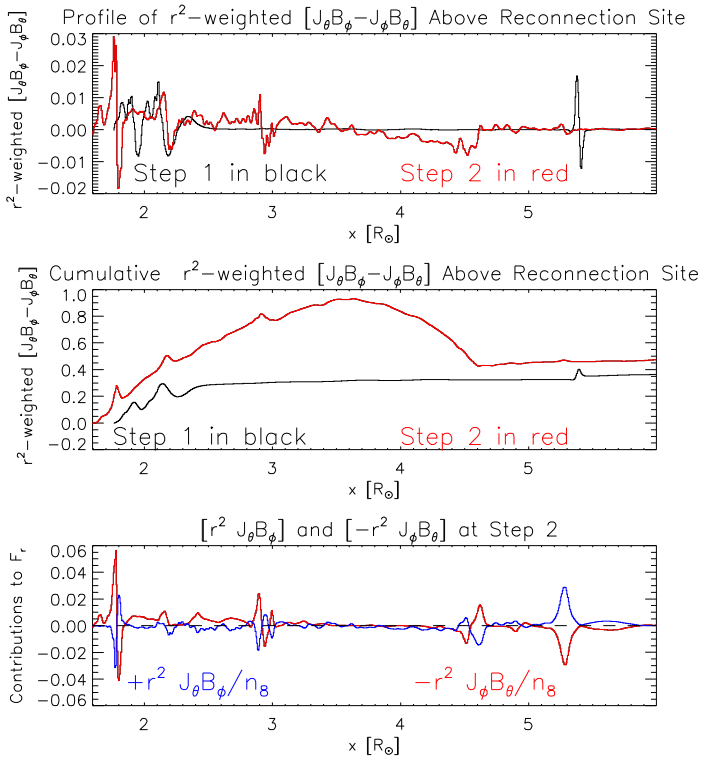

Figure 4. Top: Black (red) curves show r^2-weighted contributions to the radial Lorentz force at Step 1 (Step 2), averaged over a strip 100 cells (0.58 $R_\odot$) wide in z, outward in x from the reconnection site at that Step. Middle: Cumulative sum of the curves in the top panel from the reconnection site to each x. The excess outward force in Step 2 compared to Step 1 arises almost entirely from the diagonal, blue bands in Figure 3 just inside the CME mask around $x \in [2.5, 3.5] R_\odot$. Flank currents (see text) flow out of the page in these bands (parallel to the flare-reconnection current sheet). Bottom: For Step 2, the blue curve shows $[r^2 J_\theta B_\phi]$ and the red curve shows $[-r^2 J_\phi B_\theta]$. The latter generally makes a greater contribution to the outward Lorentz force.

accord with those reported by Jiang et al. (2021) in their analysis of another CME simulation (see bottom row of their Fig. 4). Contrary to the prediction of the flux accretion model, we see little evidence of additional hoop force from reconnected flux driving further acceleration. This conclusion, however, should not be hastily generalized to other configurations, for two reasons, both related to this simulation's axisymmetry: this model's reconnection jet is probably stronger than that in real, 3D events; and this model's hoop force is likely weaker than that in shorter-length-scale systems. Regarding the reconnection jet: the axial invariance here implies that flow and magnetic structures created in the reconnection process are coherent over much longer length scales than would be expected in a more realistic 3D geometry, within which reconnection would likely be patchy (Linton and Longcope 2006; Linton et al. 2009), producing a much more fragmented structure in the outflow. Regarding the erupting system's

length scale: the axisymmetry here implies that the radius of curvature of the model ejection's axis, r_c, is on the order of the Sun's radius, $r_c \sim R_\odot$. This might be an apt model for the eruption of a polar-crown filament, but does not accurately represent the much smaller r_c expected for an ejection from an active region, for which $r_c \sim R_\odot/10$ would often be more appropriate. Because the strength of the hoop force increases steeply for fixed ejection width as r_c shrinks (e.g., Figure 6 in Welsch 2018), a much smaller r_c should, all else equal, yield a much larger hoop force.

We conclude with recommendations for future work. In the simulation that we analyzed, the forces from the reconnection jet have deformed the eruption's core, making its trailing edge concave. We are unaware of observational reports of such concave structure within CMEs; if found, this would indicate that forces in the reconnection outflow play a substantial role in the interior structure of CMEs. Given the considerations in the two preceding paragraphs, we believe that analysis of the evolution of Lorentz forces in fully 3D, active-region-scale simulations is warranted. We also note that, while the association between CME speeds $v_{\rm CME}$ and reconnection fluxes $\Phi_{\rm rec}$ for eruptive flares is relatively well established, the flux accretion model's prediction, per the scaling in Equation (1), that CMEs' accelerations (and probably their final speeds) should be correlated with coronal magnetic field strengths in their source regions, $B_{\rm CME}$, has not been tested. We suggest that potential-field extrapolation might be an easy approach to test this prediction, but note that radio observations might enable direct estimation of $B_{\rm CME}$.

Acknowledgements. We thank the U.S. taxpayer, whose taxes helped support the work performed here. We thank B. J. Lynch for supplying code to read this ARMS output into IDL, and for taking the time to write a detailed how-to for executing this conversion. BTW is also grateful to M. Linton and B. Kliem for their time spent in engaging discussions of forces acting on CMEs. BTW gratefully acknowledges support from NASA HSR-80NSSC23K0092 and NSF SHINE AGS-2302697. CRD was supported by a grant from NASA's H-ISFM program to Goddard Space Flight Center.

References

Antiochos, S. K., DeVore, C. R., & Klimchuk, J. A. 1999, A Model for Solar Coronal Mass Ejections. *The Astrophysical Journal*, 510, 485–493.

Chae, J. 1999, Non-Coplanar Magnetic Reconnection as a Magnetic Twist Origin. *Journal of Korean Astronomical Society*, 32(2), 137–147.

Chen, J. 1996, Theory of prominence eruption and propagation: Interplanetary consequences. *Journal of Geophysical Research*, 101(10), 27499–27520.

Falconer, D. A. 2001, A prospective method for predicting coronal mass ejections from vector magnetograms. *Journal of Geophysical Research*, 106, 25185–25190.

Falconer, D. A., Moore, R. L., & Gary, G. A. 2003, A measure from line-of-sight magnetograms for prediction of coronal mass ejections. *Journal of Geophysical Research (Space Physics)*, 108, 1380.

Gopalswamy, N., Yashiro, S., Akiyama, S., & Xie, H. 2017, Estimation of Reconnection Flux Using Post-eruption Arcades and Its Relevance to Magnetic Clouds at 1 AU. *Solar Physics*, 292, 65.

Hagyard, M. J., Teuber, D., West, E. A., & Smith, J. B. 1984, A quantitative study relating observed shear in photospheric magnetic fields to repeated flaring. *Solar Physics*, 91, 115–126.

Jiang, C., Feng, X., Liu, R., Yan, X., Hu, Q., Moore, R. L., Duan, A., Cui, J., Zuo, P., Wang, Y., & Wei, F. 2021, A fundamental mechanism of solar eruption initiation. *Nature Astronomy*, 5, 1126.

Karpen, J. T., Antiochos, S. K., & DeVore, C. R. 2012, The Mechanisms for the Onset and Explosive Eruption of Coronal Mass Ejections and Eruptive Flares. *The Astrophysical Journal*, 760, 81.

Kliem, B. & Török, T. 2006, Torus Instability. *Physical Review Letters*, 96(25), 255002–+.

Lin, J. & Forbes, T. G. 2000, Effects of reconnection on the coronal mass ejection process. *Journal of Geophysical Research*, 105(A2), 2375–2392.

Linton, M. G., DeVore, C. R., & Longcope, D. W. 2009, Patchy reconnection in a Y-type current sheet. *Earth, Planets, and Space*, 61, 573–576.

Linton, M. G. & Longcope, D. W. 2006, A Model for Patchy Reconnection in Three Dimensions. *The Astrophysical Journal*, 642, 1177–1192.

Longcope, D. W., Ravindra, B., & Barnes, G. 2007, Determining the Source of Coronal Helicity through Measurements of Braiding and Spin Helicity Fluxes in Active Regions. *The Astrophysical Journal*, 668, 571–585.

McKenzie, D. E. Signatures of Reconnection in Eruptive Flares. In Martens, P. C. H. & Cauffman, D., editors, *Multi-Wavelength Observations of Coronal Structure and Dynamics* 2002,, volume 13 of *COSPAR Colloq. Series*, pp. 155–164.

Moore, R. L., Sterling, A. C., Hudson, H. S., & Lemen, J. R. 2001, Onset of the Magnetic Explosion in Solar Flares and Coronal Mass Ejections. *ApJ*, 552, 833–848.

Petschek, H. E. Magnetic Field Annihilation. In *NASA Special Publication* 1964,, volume 50, 425.

Priest, E. R. & Forbes, T. G. 2000,. *Magnetic reconnection: MHD theory and applications*. Cambridge University Press, New York.

Qiu, J. & Yurchyshyn, V. B. 2005, Magnetic Reconnection Flux and Coronal Mass Ejection Velocity. *The Astrophysical Journal Letters*, 634, L121–L124.

Welsch, B. T. 2018, Flux Accretion and Coronal Mass Ejection Dynamics. *Solar Physics*, 293(7), 113.

Wright, A. N. & Berger, M. A. 1989, The effect of reconnection upon the linkage and interior structure of magnetic flux tubes. *Journal of Geophysical Research*, 94(A2), 1295–1302.

Zhang, J. & Dere, K. P. 2006, A Statistical Study of Main and Residual Accelerations of Coronal Mass Ejections. *The Astrophysical Journal*, 649, 1100–1109.

Discussion — Questions & Responses

Question, by Dr. Bernhard Kliem: It appears possible that the increase of the outward hoop force from the flux accretion to the erupting rope by flare reconnection underneath is weaker than estimated so far, because this flux carries little current. The currents driving the accretion of the flux flow in the slow-mode shocks attached to the diffusion region (or to the uppermost diffusion region if several such regions exist). The Lorentz force of these currents accelerates the upward reconnection outflow jet, hence, drives the accretion of flux to the erupting flux rope. The new flux itself carries little current; it "dipolarizes" while joining the rope flux. Therefore, it appears possible that the primary addition to the upward forces consists in the momentum transfer from the upward reconnection jet to the erupting flux rope (if the jet moves faster than the rope). There is no doubt on the reduction of the downward tension force of overlying flux by flare reconnection. This latter effect is included in the treatment of the torus instability by Kliem and Török (2006).

Response, by Dr. Welsch: Regarding the presence of currents in the outflow region, the flux accretion model does indeed posit that the post-reconnection flux *dipolarizes* (e.g., Priest and Forbes 2000) — i.e., evolves toward a roughly dipolar shape. But only an exactly dipolar field is current-free; we may sensibly speak of a compressed or stretched dipolar field, which contains currents, but is still essentially dipolar in character (versus unipolar or quadrupolar). Thus, I do not use the term "dipolarization" to imply that significant currents are not present. (This term appears to have originally been applied to retraction of highly stretched magnetotail fields in geospace toward the Earth after reconnecting; but even when fully dipolarized, these fields form a stretched dipole.)

Clearly, however, we did not find evidence of the outward hoop force acting in the simulation analyzed here. However, as noted in the concluding section of this article (above), compared to the solar case, this simulation's axisymmetry probably makes both (1) the reconnection jet stronger and (2) the hoop force weaker. Hence, determining whether the hoop force from post-reconnection magnetic fields is dynamically important or not requires analysis of other models with more realistic geometry.